J Solid State Electrochem (2010) 14:1915–1922
DOI 10.1007/s10008-010-1024-x

ORIGINAL PAPER

Tunable activity in electrochemical reduction of oxygen by gold–polyaniline porous nanocomposites

Jixia Song · Junhua Yuan · Fei Li · Dongxue Han · Jiangfeng Song · Li Niu

Received: 26 September 2009 / Revised: 19 December 2009 / Accepted: 4 February 2010 / Published online: 9 March 2010

Abstract Oxygen electrochemical reduction on gold–polyaniline (Au–PANI) porous nanocomposite-modified glassy carbon electrode in basic media was described. The as-prepared Au–PANI porous nanocomposite showed superior tunable activity for electrochemical reduction of oxygen. The specific surface area of Au–PANI porous nanocomposites was evaluated to be about 11.3 m^2g^{-1} through a convenient voltammetric approach. Rotating ring-disk electrode experiments further demonstrated the number of electrons exchanged in oxygen reduction increased from 2e to 4e with increasing the trigger potential from 300, to 500, 700 mV. The tunable activity in electrochemical reduction of oxygen was achieved as a result of positive potential-induced formation and reduction of Au surface oxide. However, the tunable oxygen reduction reaction is fit for applying potential in a linear positive-going potential sweep. Irreversible ORR tunability was found after a more active surface formed at 700 mV. To optimize the applied potential window on these Au-based porous materials has potential applications such as in electrochemical sensing, fuel cells, or getting rid of the interference from the coexisted substances.

Keywords Porous material · Gold–polyaniline nanocomposites · Oxygen reduction reaction · Tunable electrocatalysis · Gold oxide

Abbreviations

ORR	Oxygen reduction reaction
Au–PANI	Gold–polyaniline
GCE	Glassy carbon electrode
RRDE	Rotating ring-disk electrode
PANI	Polyaniline
Au	Gold
NADH	β-nicotinamide adenine dinucleotide
GOx	Glucose oxidase
Au–PANI/GCE	Au–PANI porous nanocomposites-modified electrode
SDS	Sodium dodecyl sulfate
APS	Ammonium peroxydisulate
CV	Cyclic voltammetry
EIS	Electrochemical impedance spectroscopy

Introduction

Nanostructured gold (Au) shows good performances toward catalysis or electrochemical catalysis due to its high surface-to-volume ratio. Tailoring shape or morphology of gold nanostructures has attracted considerable attention, owing to their tunable electronic, optical, magnetic, and catalytic properties and corresponding to various fields of applications [1–6]. Thus, efforts were devoted to the preparation of gold with versatile shapes [7–14]. Additionally, nanoporous gold had an unexpectedly high catalytic activity for CO oxidation [15] and reduction of H_2O_2 [16]. Dealloying [17–19] was used as a general route for fabricating nanoporous Au, which involves the application of toxic agent such as CN^- or corrosive concentrated HNO_3. Accordingly, greener and

Junhua Yuan and Li Niu contributed equally to this study.

J. Song · J. Yuan · F. Li · D. Han · J. Song · L. Niu (✉)
State Key Laboratory of Electroanalytical Chemistry,
Changchun Institute of Applied Chemistry,
Changchun 130022, People's Republic of China
e-mail: lniu@ciac.jl.cn

J. Song · J. Yuan · F. Li · D. Han · J. Song · L. Niu
Chinese Academy of Sciences,
Graduate University of the Chinese Academy of Sciences,
Changchun 130022, People's Republic of China

J. Yuan (✉)
College of Chemistry and Life Science,
Zhejiang Normal University,
Jinhua 321004, China
e-mail: jhyuan@zjnu.cn

simpler method for the synthesis of nanoporous Au was attempted to meet the need [16].

Polyaniline (PANI) is one of the most important conducting polymers because of its facile preparation, tunable conductivity, and high environmental stability. Composites containing PANI and gold have received a great deal of attention because of their unique electronic and optical properties as well as extensive applications in diverse areas. In particular, it was reported that PANI/Au multilayers [20] could electrochemically catalyze the oxidation of β-nicotinamide adenine dinucleotide (NADH) and detect DNA. PANI/Au hollow spheres [21] showed enhanced bioelectrocatalytic activity for oxidation of dopamine and higher electronic conductivity compared with pure PANI hollow spheres. In addition, PANI/Au nanoparticles composites have been used as electron-transfer mediators for the bioelectrocatalytic activation of glucose oxidase toward the oxidation of glucose [22]. The oxygen reduction reaction (ORR) [23–27] is one of the typical systems for measuring the catalytic properties and of great importance for fuel cell investigations. However, reports on tuning the catalytic activity for ORR are still very few [26, 28]. Although PANI/Au composites have been widely studied, it has not been reported that PANI/Au nanocomposites with tunable activity of electrochemical reduction of oxygen in basic media.

Here, the Au–PANI porous nanocomposites were fabricated according to our previous work. The specific surface area of the Au–PANI nanocomposites was estimated ca. 11.3 $m^2 g^{-1}$ through voltammetric approach based on the amount of charge consumed during the reduction of the Au surface oxide. The resulting Au–PANI porous nanocomposites-modified electrodes (Au−PANI/glassy carbon electrode (GCEs)) were applied for the ORR in basic media. By applying a positive-going initial potential to the modified electrode, the resulting Au–PANI/GCEs revealed superior tunable oxygen reduction reaction activity. Au oxidation from the triggering potential and the synergistic effect of porous Au and PANI in the nanocomposites played key roles. Moreover, irreversible ORR tunability was found after a more active surface generated at 700 mV.

Experimental

Chemicals and synthesis

Before use, aniline was distilled at reduced pressure and kept below 0 °C. Chloroauric acid ($HAuCl_4 \cdot 3H_2O$), sodium dodecyl sulfate (SDS), ammonium peroxydisulate (APS), H_3PO_4, NaOH, K_4 [Fe $(CN)_6$], K_3 [Fe $(CN)_6$], and KCl were analytical grade and were used as received. The Au−PANI porous nanocomposites were prepared according to our previous work [29]. Briefly, 0.0167 g SDS was added to 5 mL 0.1 mol L^{-1} H_3PO_4 solution containing 0.01 mol L^{-1} aniline. The solution was ultrasonic agitated till SDS was entirely dissolved. Then, 1.0 mL 15 mmol L^{-1} $HAuCl_4$ solution was further added dropwise and kept stirring overnight at room temperature. The browny green precipitate was collected and washed with water, ethanol, and *N*-methyl-pyrrolidone via centrifugation, respectively.

In control experiments, PANI was polymerized via adding 1 mL 0.4 mol L^{-1} APS to 5 mL solution containing 0.01 mol L^{-1} aniline and 0.1 mol L^{-1} H_3PO_4 and stirring overnight. The green precipitate was rinsed with water, methanol *N*-methyl-pyrrolidone through centrifugation, respectively. The gold nanoparticles were prepared according to Frens's report [7]. Briefly, 0.5 mL sodium citrate (1% by weight) was added into 50 mL boiling gold chloride (0.01% by weight). The wine red color solution was cooled into room temperature after 5 min reduction. Mix the obtained Au nanoparticles and PANI physically and centrifuged to form a 0.5 mg/mL of dispersion.

All glassware used in the preparation of Au-related nanomaterials was soaked with freshly prepared aqua regia (extreme care due to its powerful oxidative activity) and washed thoroughly with water.

Characterizations

Transmission electron microscopy (TEM) images were obtained using a Hitachi H-8100 transmission electron microscope operated at 200 kV. TGA data were collected on Pyris Diamond TG/DTA (PE, America). The samples were heated from 40 to 700 °C at a rate of 10 °C/min under air atmosphere. Cyclic voltammetric (CV) measurements were performed in a conventional three-electrode cell with a coiled platinum wire as the counter electrode and an Ag|AgCl (in saturated KCl) as the reference electrode on a CHI 660a electrochemical workstation (CHI, USA). The working electrode was bare or chemical-modified glassy carbon electrode (d=3 mm). An EG & PARC model 636 rotating ring-disk electrode (RRDE) system and an EG & PARC model 366 bipotentiostat were used for rotating ring-disk voltammetry experiments. A rotating glassy carbon disk–platinum ring electrode with a disk diameter of 5 mm was used as working electrode. The collection efficiency (N) of the ring electrode obtained by reducing ferricyanide at a disk electrode was 0.139. Electrochemical impedance spectroscopy (EIS) were performed with a Solartron 1470 battery test unit and a Solartron 1255B frequency response analyzer (Solartron Inc., England) for 1 mM K_4 [$Fe(CN)_6$] + 1 mM K_3[$Fe(CN)_6$] in 0.1 M KCl aqueous solution. A sinusoidal potential modulation of ±5 mV amplitude was superimposed on the open-circuit potential. Applied frequency was from 10^5 to 0.01 Hz.

The as-washed precipitate was dispersed in ethanol, and then a small amount of the ethanol suspension was dropped and evaporated slowly in ambient on a carbon-coated copper grids for TEM imaging. For electrochemical measurements, a total of 15 μL of 0.5 mg/mL water dispersed precipitate was cast on the freshly polished GCE and 30 μL for glassy carbon disk–platinum ring electrode and allowed to dry overnight in ambient. Another 10 μL of 0.5% of Nafion was cast on the modified disk-ring electrode for stability and dried. The modified GCE was denoted as Au– PANI/GCE. The conventional PANI modified and mixture of gold nanoparticles and PANI-modified GCE were prepared following similar procedures to the above Au–PANI/GCE and named as PANI/GCE and Au+P/GCE, respectively. The nitrogen-saturated and oxygen-saturated solutions were prepared by bubbling the electrolytes with pure N_2 or ultrahigh purity oxygen through the electrolyte solution for at least 15 min, respectively.

Results and discussions

Physical characterization of Au–PANI composites

The resulted Au–PANI composites dispersed in distilled water are light green in color, as seen the photos in Fig. 1a, which is indicative of the existence of PANI. Figure 1b is the digital picture of the centrifuged and dried resultants adsorbed on the plastic centrifuge tube. See from the outside of the tube, it exhibits brown color with metal luster. TEM image (Fig. 1c) shows that the resulting nanocomposites depict an appearance in shape of microsheets with ca. 3~ 42 nm in width of nanopores. The contrast along the edges shows that the Au core is enwrapped with ca. 8-nm-thick shell of polymer, as marked in Fig. 1c. Thermal properties of PANI and Au–PANI porous nanocomposites were measured in air atmosphere to investigate the components of the materials obtained. Figure 1d represents the TGA curves of PANI prepared with conventional APS oxidation reaction (dotted line) and Au–PANI porous nanocomposite (solid line). It is observed that there is a typical three-step weight-loss behavior of PANI in Fig. 1d dotted line: first loss of water or solvent followed by the second loss of dopant and low molecular weight fragments of the polymer. And the final loss results from the oxidative degradation and decomposition of the polymer backbone [30]. Heating Au–PANI porous nanocomposites in air also represents the three-step weight loss of PANI, but only lost 3% in the whole process and left 97% Au component (Fig. 1d, solid line). It provides evidence that PANI existed in small weight percentage in the Au–PANI porous nanocomposites while Au was in a dominant percentage.

Electrochemical characterization of Au–PANI nanocomposites

In order to get surface information about the Au porous material in Au–PANI/GCE, 6 μL of 1 mg mL^{-1} Au–PANI nanocomposites dispersion was cast onto the surface of GCE. After drying in ambient for 12 h, cyclic voltammetry were recorded in 0.5 mol L^{-1} H_2SO_4 solution in the potential range from −100 to 1,650 mV (vs. Ag|AgCl) with the scan rate of 100 mV s^{-1}. The reduction peak during the cathodic sweep was used for calculation as revealed in Fig. 2. Based on the amount of charge consumed during the reduction of the Au surface oxide monolayer and a previously reported reference value of 400 μC cm^{-2} was used for the calculation [16, 31–33] according to the two equations [31], the specific

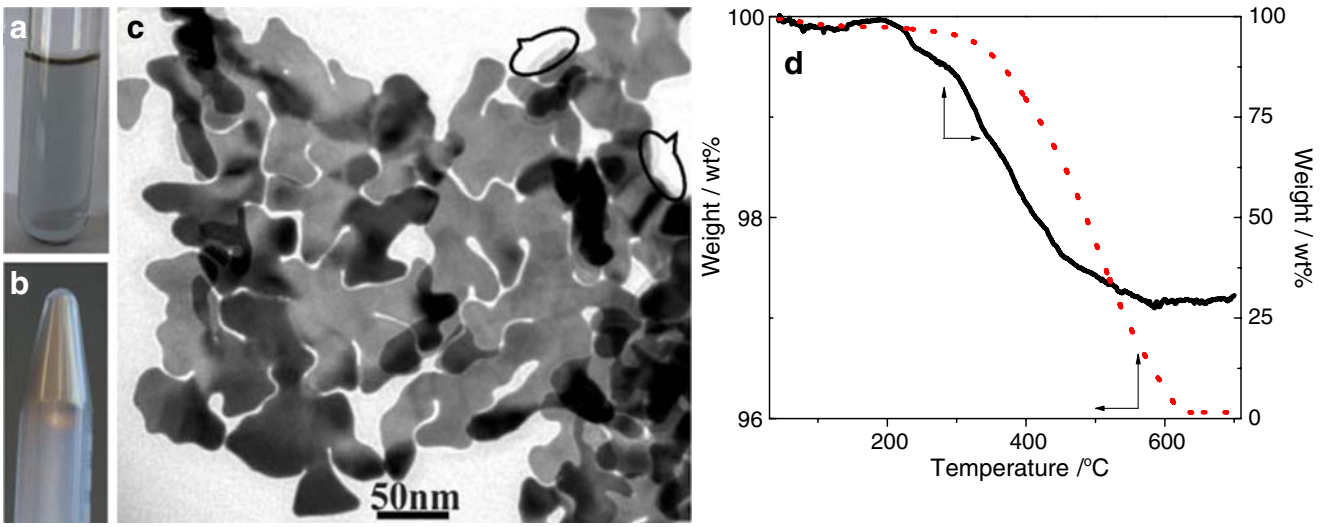

Fig. 1 Photographs (**a** dispersion and **b** dry film) and TEM image (**c**) of Au–PANI porous nanocomposites, **d** TGA curves of PANI (*dotted line*) and Au–PANI porous nanocomposites (*solid line*)

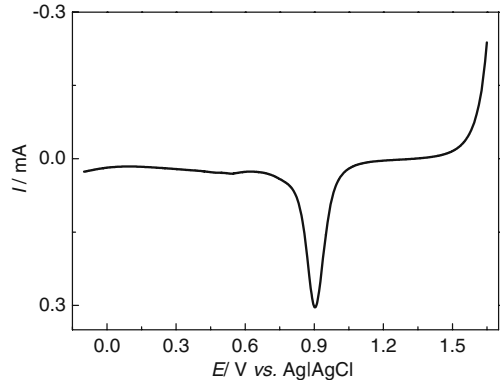

Fig. 2 Voltammogram of Au–PANI/GCE with the potential range of −100~1,650 mV in 0.5 mol L^{-1} H_2SO_4 solution. Scan rate, 100 mV s^{-1}

surface area of the Au–PANI nanocomposites loading on GCE is estimated about 11.3 m^2g^{-1}, which is higher than the previous report (i.e., 8.2 m^2g^{-1}) [19].

$$\tau C = \mathrm{d}Q \Big/ \mathrm{d}E = I\mathrm{d}t \Big/ \mathrm{d}E = I \Big/ (\mathrm{d}E/\mathrm{d}t) \quad (1)$$

$$A = \tau C \Big/ C^* \quad (2)$$

Where τC is the total capacitance, Q is charge, E is potential, I is current, t is time, A is the surface area, and C^* is a reference value.

Tunable electrochemical reduction of O_2 at Au–PANI nanocomposites

With the aim at exploring the electrochemical activity of the Au–PANI for ORR, the Au–PANI/GCEs were studied using cyclic voltammetry in 0.1 mol L^{-1} NaOH aqueous solution. The scanning potential started from a certain positive point: 100, 300, 400, 500, and 700 mV, respectively, to a settled negative potential −600 mV. Figure 3 shows each five sets of cyclic voltammetric curves of Au–PANI/GCE starting at successive series of increasing positive potentials in (a) O_2- and (b) N_2-saturated 0.1 mol L^{-1} NaOH solution. The arrows indicate the direction of the potential scan. Both in O_2-saturated and N_2-saturated 0.1 mol L^{-1} NaOH solution, when the potential limit was 400 mV (curve C), it was accompanied by a large reduction wave at ca. 100 mV. And when widening the potential window to 500 mV (curve D) and even to 700 mV (curve E), the reduction waves got better resolved. It was due to the removal of oxide formation on the gold surface [34, 35]. As revealed in Fig. 3a in presence of O_2, with increasing the initial potential, from curve A to curve E, the corresponding reduction potential of O_2 tunes positively from −413, −410, −310, −247, to −184 mV as well as the reduction current increase. The obviously increased peak current and positive shift in peak potential suggests that such Au–PANI nanocomposites exhibit highly tunable electroreductive activity for O_2. This could be attributed to the influence of the formation of surface gold oxides [34, 35]. OH^- anions in the alkaline solutions firstly adsorbed on the Au–PANI nanocomposite electrode and generated surface Au oxides. While, surface Au oxides would be electrochemically reduced to Au in the vicinity of 0.1 V at backward potential scan [36, 37]. Subsequently, the Au electrochemical catalyzed O_2 at the more negative potential. The more positive potential applied, the more surface Au oxides formed, which is more beneficial to O_2 reduction.

Electrochemical reduction of O_2 at bare GCE, PANI, and mixture of Au nanoparticles and PANI

To investigate the influences of morphology on the tunable electrochemical reductions toward oxygen, the subsequent

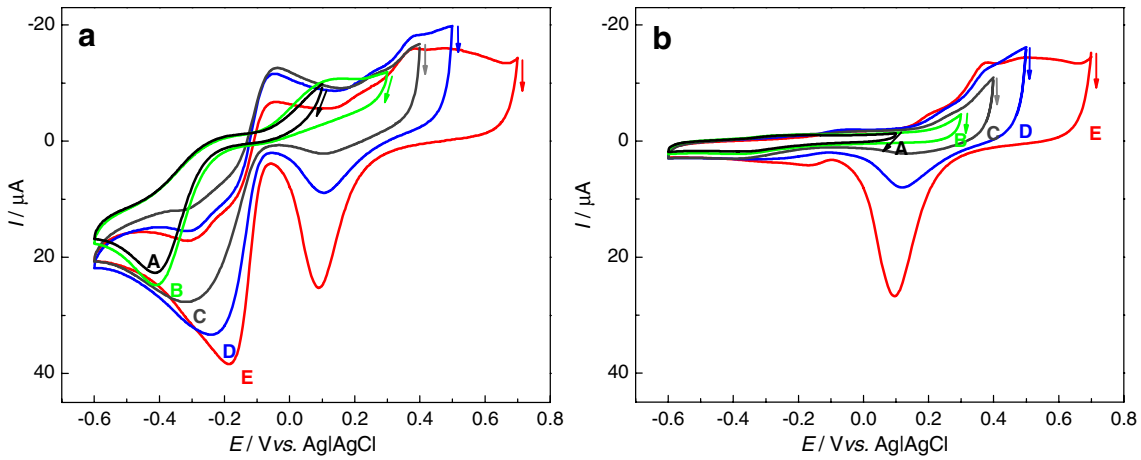

Fig. 3 Cyclic voltammograms of Au–PANI/GCE in (**a**) O_2- and (**b**) N_2-saturated 0.1 mol L^{-1} NaOH solution. *A* 100~−600 mV, *B* 300~−600 mV, *C* 400~−600 mV, *D* 500~−600 mV, *E* 700~−600 mV. Scan rate, 50 mV s^{-1}

three control experiments were carried out. Firstly, cyclic voltammetry was applied at bare GCE in O_2-saturated 0.1 mol L^{-1} NaOH solution, as shown in Fig. 4a, the corresponding O_2 reduction waves behaves in an opposite manner to Au–PANI, which shifts negatively from −310 to −425 mV with increasing of the starting point from 100, 300, and 400 to 500 mV (curve A to D). Especially the initial potential is settled from 700 mV, the reductive peak disappears obviously (curve E).

PANI was polymerized the APS as oxidant and yielded as fibers of 20 nm in diameter on average (inset of Fig. 4b). The PANI fiber-modified GCE (PANI/GCE) was also examined side-by-side by CV measurements in 0.1 mol L^{-1} O_2-saturated NaOH solution. As revealed in Fig. 4b, the reductive waves are almost around ca. −430 mV (curve A to C). When the starting potential is set as 500 mV, only slight negative shift is observed in curve D. While further widening the potential window to 700~−600 mV (curve E), the PANI/GCE shows a similar behavior to the bare GCE. It is well known that PANI film does not have electrochemical activity in alkaline solution. This reduction of O_2 could be attributed only to the contribution of bare GCE, but hindered by the cast PANI film.

Gold nanoparticles were prepared through previous Frens's method [7]. Disperse the Au nanoparticles into the synthesized PANI fibers and make a 0.5 mg/mL of dispersion. The aggregated PANI fibers were decorated with the obtained Au nanoparticles of ca. 24 nm in diameter in sphere and ellipsoid (inset of Fig. 4c). The mixture was drop-coated on the GCE and the resulting mixture-modified GCE (Au+P/GCE) was measured in O_2-saturated 0.1 mol L^{-1} NaOH solution at different starting potentials. See from the CV curves in Fig. 4c, the peak current of ORR enhanced with increasing the scanning potentials from curve A to E, respectively. However, no reduction potential shift was observed. It proved the porous morphology and the synergistic effect of Au and PANI in the composites on the tunability of ORR to some extent.

RRDE for oxygen reduction reaction at Au–PANI nanocomposites

In basic media, generally, oxygen electroreduction can proceed in two different pathways [38]: the direct four-electron reduction proceeds as

$$O_2 + 2H_2O + 4e^- \rightarrow 4OH^- \quad (3)$$

While peroxide-intermediate-based the two-electron pathway can be expressed as follows:

$$O_2 + H_2O + 2e^- \rightarrow HO_2^- + OH^- \quad (4)$$

$$HO_2^- + 2e^- + H_2O \rightarrow 3OH^- \quad (5)$$

For further proof of higher reactivity on positive potential polarization, a rotating ring-disk electrode technique was employed to obtain the number of electrons associated with the O_2 reduction process on porous Au–PANI in 0.1 mol L^{-1} NaOH solution. As shown in Fig. 5, the GC disk potential was scanned from 300 mV (a, d), 500 mV (b, e), and 700 mV (c, f) to −600 mV while the platinum ring potential was held at 650 mV to oxidize the H_2O_2 generated by O_2 reduction at the disk electrode. For each electrode potential window, $1/i$ has a linear relationship with $\omega^{-1/2}$ to follow the Koutecky–Levich equation [39]:

$$\frac{1}{i} = \frac{1}{i_k} + \frac{1}{0.62nFAD_o^{2/3}\omega^{1/2}\nu^{-1/6}C_o} \quad (6)$$

where i_k is the kinetic current in the absence of mass-transfer effect; n is the number of electrons exchanged in the O_2 reduction reaction; F is the Faraday constant; A is electrode area; D_o is the diffusion coefficient of O_2 (1.9×10^{-5} cm^{-1}); ω is the rotating rate; ν is the kinematic viscosity (9.97×10^{-5} $cm^2 s^{-1}$), and C_o is the bulk concentration of O_2 (1.38×

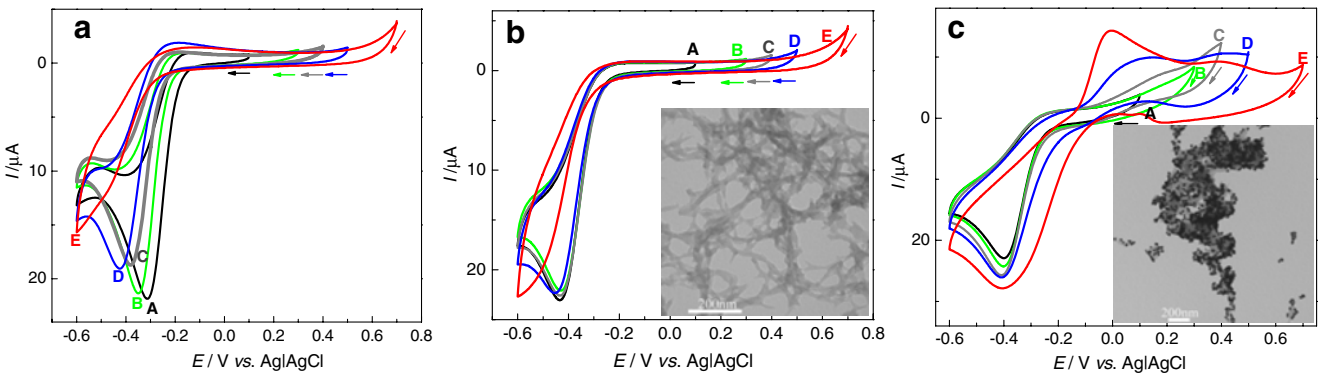

Fig. 4 Cyclic voltammograms of **a** bare GCE, **b** PANI/GCE, **c** Au+P/GCE in O_2-saturated 0.1 mol L^{-1} NaOH solution (*A*~*E*) with different potential range: (*A*) 100~−600 mV, (*B*) 300~−600 mV, (*C*) 400~−600 mV, (*D*) 500~−600 mV, (*E*) 700~−600 mV. Scan rate, 50 mV s^{-1}. TEM images of PANI and Au+P are shown as *inset* of **b** and **c**, respectively

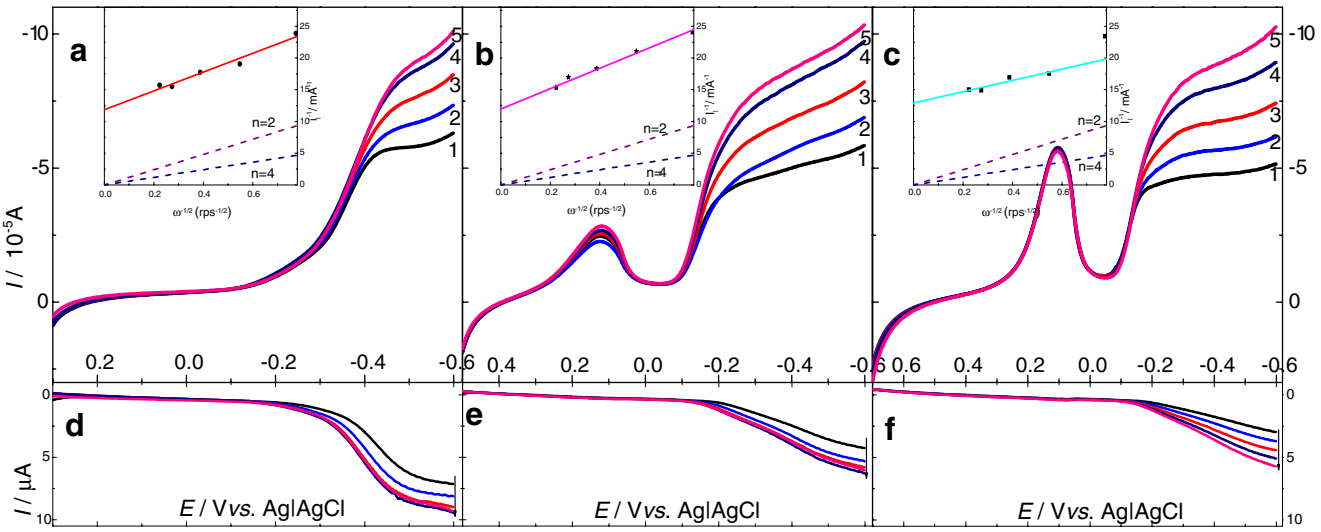

Fig. 5 Rotating ring-disk electrode voltammograms obtained from porous Au–PANI surfaces in O_2-saturated 0.1 mol L^{-1} NaOH solution with different potential range: **a**, **d** 300~−600 mV; **b**, **e** 500~−600; **c**, **f** 700~−600 mV. The rotating rate was varied from (*1*) 100, (*2*) 200, (*3*) 400 to (*4*) 800, and (*5*) 1,200 rpm. Scan rate, 50 mV s^{-1}. The potential of the platinum ring electrode was set to 650 mV in order to oxidize H_2O_2 to O_2. Each *inset* is Koutecky–Levich plots obtained from corresponding potentials windows. The *solid line* is fitted from the experimental data, and the *dashed lines* are from the calculated data considering the reduction of O_2 by two and four electrons, respectively

10^{-6}mol cm^{-3}) [38]. Take the potential window of 300~−600 mV and rotating rate of 1,200 rpm (Fig. 5a, d) for example firstly, the ratio of the ring to disk current, i_R/i_D, is 0.11 for the porous Au–PANI-modified electrode. The calculated number of electrons involved in the reduction of O_2 is found to be 2.4 according to the equation $n = 4 - 2 \times \frac{i_R}{i_D N}$ $(N = 0.139)$ [40]. The n value suggests that O_2 reduction on porous Au–PANI surface in 0.1 mol L^{-1} NaOH solution is nearly 2e process to yield HO_2^-, which confirms the result acquired from the Koutecky–Levich plot as shown in the inset of Fig. 5a.

In the same way, the n values were calculated to be 3.2 in scanning window of 500~−600 mV (i_R/i_D=0.054) and up to 3.5 with initial potential at 700 mV (i_R/i_D=0.037) as a nearly a four-electron process to produce OH^-. It indicates the initial positive potential-dependent kinetic behavior of the O_2 electrochemical reduction.

Irreversibility of tunable ORR activity at Au–PANI nanocomposites

It is reported [34] that the oxidation region of Au arose at 0.6 to 0.8 V in alkaline solutions, depending on pH. Irreversible behavior of formation and reduction of oxide films at noble metals were also previously adopted. Thus, the reproducibility of the Au oxide formation and reduction-related tunability of ORR was the concern in our present research. Figure 6a shows CVs of Au–PANI nanocomposites-modified electrode in 0.5 mol L^{-1} H_2SO_4 at the before and after the series of ORRs. A positive shift of reduction peak and a more negative onset of oxidation potential are observed at the Au–PANI/GCE. After electrocatalyzing O_2 reduction, more gold oxide formed and reduced result in the more active surface maintained [41]. EIS can provide useful information on the impedance changes of the electrode surface. The high-

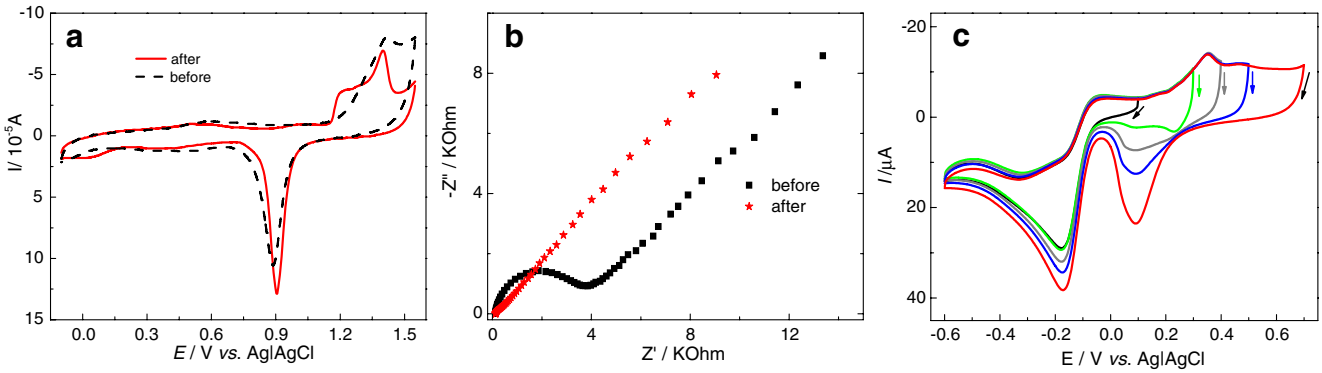

Fig. 6 **a** CV curves in 0.5 M H_2SO_4 and **b** Nyquist diagrams in 1 mM K_4 [Fe(CN)6] + 1 mM K_3[Fe(CN)$_6$] in 0.1 M KCl aqueous solution at open-circuit potential of Au–PANI/GCE before and after a series of ORRs in O_2-saturated 0.1 mol L^{-1} NaOH solution. **c** Another set of ORR CV grams after finishing scanning within the above different potential ranges. Scan rate, 50 mV s^{-1}

frequency region is usually associated with the kinetics of the faradaic process, and the low-frequency region contains information regarding the diffusion of the species to the electrode surface. The Nyquist diagrams of Au–PANI/GCE before and after electrocatalysis were measured at different open-circuit potentials (Fig. 6b). A very large semicircle in the high-frequency region was observed at fresh Au–PANI-modified GCE (squares). In contrast, the semicircle switched much smaller after the above series of ORR scanning finished (stars), this promoted electron-transfer kinetics [42, 43] indicated more surface active was achieved by repeated ORR cycling. The ORR activity increased with the higher upper potential. However, once an oxide film has been formed on Au at a higher given potential, the reductive peak of O_2 switched to a more positive potential rather than recover to its original potential at the repeated lower upper limit. Another series of ORR was repeated after the CV scanning finished within the above different potential ranges. No remarkable tunable activity was observed in the following CV grams in Fig. 6c. However, a similar potential peak for ORR located at about −180 mV. So the tunable oxygen reduction reaction is suitable for applying potential in a linear positive-going direction. From another aspect, a more active surface gave rise to a more favorable ORR once the Au oxide formed extensively.

Conclusions

In summary, the Au–PANI porous nanocomposites-modified electrode shows high tunable activity on electrochemical reduction toward O_2 by tuning the initial potential in 0.1 mol L^{-1} NaOH solution. Rotating ring-disk electrode voltammetry and Koutecky–Levich plots quantitatively proved the applied initial scanning potential influenced the pathway involved in the reduction of O_2 in basic media. Therefore, quantitative and qualitative results further confirmed both the trigger potential-related formation and reduction of Au surface oxide and the synergistic effects of porous Au and PANI in the nanocomposites were significant parameters to control the tunable electrochemical activity for ORR. However, irreversibility of tunable ORR activity was found after a more active surface formed at 700 mV. The tunable oxygen reduction reaction is limited for applying potential in a linear positive-going potential sweep and the upper potential limit is not greater than 700 mV. These porous nanocomposites could offer a possibility to apply the material to specific systems, such as sensors or fuel cells, with high activity and selectivity by optimizing the applied potential windows to eliminate the interference from the coexisted substances.

Acknowledgments The authors appreciate the useful discussions with Dr. Y. Zhang, Dr. Y. Shen, and J. Zhai. And we are also grateful to National Natural Science Foundation of China (NSFC, No.20903082 and 20827004) for the financial support.

References

1. El-Sayed MA (2001) Acc Chem Res 34:257
2. Grzelczak M, Perez-Juste J, Mulvaney P, Liz-Marzan LM (2008) Chem Soc Rev 37:1783
3. Jain PK, Huang X, El-Sayed IH, El-Sayed MA (2008) Acc Chem Res 41:1578
4. Murphy CJ, Gole AM, Stone JW, Sisco PN, Alkilany AM, Goldsmith EC, Baxter SC (2008) Acc Chem Res 41:1721
5. Skrabalak SE, Chen J, Sun Y, Lu X, Au L, Cobley CM, Xia Y (2008) Acc Chem Res 41:1587
6. Yan Y-M, Tel-Vered R, Yehezkeli O, Cheglakov Z, Willner I (2008) Adv Mater 20:2365
7. Frens G (1973) Nature 241:20
8. Jana NR, Gearheart L, Murphy CJ (2001) J Phys Chem B 105:4065
9. Sun XP, Dong SJ, Wang E (2004) Angew Chem Int Ed 43:6360
10. Halder A, Ravishankar N (2006) J Phys Chem B 110:6595
11. Li ZH, Ravaine V, Ravaine S, Garrigue P, Kuhn A (2007) Adv Funct Mater 17:618
12. Huo ZY, Tsung CK, Huang WY, Zhang XF, Yang PD (2008) Nano Lett 8:2041
13. Lu X, Yavuz MS, Tuan H-Y, Korgel BA, Xia Y (2008) J Am Chem Soc 130:8900
14. Huang X-J, Li C-C, Gu B, Kim J-h, Cho S-O, Choi Y-K (2008) J Phys Chem C 112:3605
15. Zielasek V, Jurgens B, Schulz C, Biener J, Biener MM, Hamza AV, Baumer M (2006) Angew Chem Int Ed 45:8241
16. Chandra D, Jena BK, Raj CR, Bhaumik A (2007) Chem Mater 19:6290
17. Ding Y, Erlebacher J (2003) J Am Chem Soc 125:7772
18. Dixon MC, Daniel TA, Hieda M, Smilgies DM, Chan MHW, Allara DL (2007) Langmuir 23:2414
19. Shulga OV, Jefferson K, Khan AR, D'Souza VT, Liu JY, Demchenko AV, Stine KJ (2007) Chem Mater 19:3902
20. Tian SJ, Liu JY, Zhu T, Knoll W (2004) Chem Mater 16:4103
21. Feng XM, Mao CJ, Yang G, Hou WH, Zhu JJ (2006) Langmuir 22:4384
22. Granot E, Katz E, Basnar B, Willner I (2005) Chem Mater 17:4600
23. Maruyama J, Inaba M, Ogumi Z (1998) J Electroanal Chem 458:175
24. Zhang YR, Asahina S, Yoshihara S, Shirakashi T (2003) Electrochim Acta 48:741
25. Tian Y, Liu HQ, Zhao GH, Tatsuma T (2006) J Phys Chem B 110:23478
26. Zhai JF, Huang MH, Dong SJ (2007) Electroanalysis 19:506
27. Sarapuu A, Nurmik M, Mandar H, Rosental A, Laaksonen T, Kontturi K, Schiffrin DJ, Tammeveski K (2008) J Electroanal Chem 612:78
28. Cheng WL, Dong SJ, Wang EK (2004) J Phys Chem B 108:19146
29. Bu X, Yuan J, Song J, Han D, Niu L (2009) Mater Chem Phys 116:153
30. Zhang LJ, Long YZ, Chen ZJ, Wan MX (2004) Adv Funct Mater 14:693
31. Trasatti S, Petrii OA (1991) Pure Appl Chem 63:711
32. Dai X, Compton RG (2006) Anal Sci 22:567
33. Soreta TR, Strutwolf J, O'Sullivan CK (2008) ChemPhysChem 9:920
34. Angerstein-Kozlowska H, Conway BE, Barnett B, Mozota J (1979) J Electroanal Chem 100:417

35. Conway BE (1995) Prog Surf Sci 49:331
36. Yu CF, Jia FL, Ai ZH, Zhang LZ (2007) Chem Mater 19:6065
37. Liu Z, Huang L, Zhang L, Ma H, Ding Y (2009) Electrochim Acta 54:7286
38. Kim JW, Gewirth AA (2006) J Phys Chem B 110:2565
39. Bard AJ, Faulkner LR (2001) Electrochemical methods fundamentals and applications, 2nd edn. Wiley, New York
40. Liu SQ, Xu JQ, Sun HR, Li DM (2000) Inorg Chim Acta 306:87
41. Campuzano S, Pedrero M, Montemayor C, Fatas E, Pingarron JM (2006) J Electroanal Chem 586:112
42. Silva TH, Garcia-Morales V, Moura C, Manzanares JA, Silva F (2005) Langmuir 21:7461
43. Zhang Y, Shen Y, Han D, Wang Z, Song J, Niu L (2006) J Mater Chem 16:4592